BNL 17767
AADD 73-3

BROOKHAVEN NATIONAL LABORATORY
Associated Universities, Inc.
Upton, New York

ACCELERATOR DEPARTMENT
Informal Report

EQUIVALENT CIRCUIT ANALYSIS OF MULTIPERIODIC STRUCTURES

W. Bauer†

February 20, 1973

†On leave of absence from IEKP, Kernforschungszentrum Karlsruhe.

NOTICE

This report was prepared as an account of work sponsored by the United States Government. Neither the United States nor the United States Atomic Energy Commission, nor any of their employees, nor any of their contractors, subcontractors, or their employees, makes any warranty, express or implied, or assumes any legal liability or responsibility for the accuracy, completeness or usefulness of any information, apparatus, product or process disclosed, or represents that its use would not infringe privately owned rights.

NOTICE
This report was prepared as an account of work sponsored by the United States Government. Neither the United States nor the United States Atomic Energy Commission, nor any of their employees, nor any of their contractors, subcontractors, or their employees, makes any warranty, express or implied, or assumes any legal liability or responsibility for the accuracy, completeness or usefulness of any information, apparatus, product or process disclosed, or represents that its use would not infringe privately owned rights.

MASTER

DISTRIBUTION OF THIS DOCUMENT IS UNLIMITED

Abstract

The effects of fabricating tolerances on rf joints in multiperiodic structures are analyzed by using an equivalent circuit description. The calculations demonstrate that the currents at the joints between single sections of a multiperiodic structure are of the same order of magnitude as in the $\pi/2$-mode structure.

I. Introduction

In a previous note[1] an equivalent circuit formalism was introduced, which allowed to analyze the questions of fabrication tolerances and joint-currents in $\pi/2$-mode structures. According to the growing interest in multiperiodic, π-mode-like structures[2] it seemed desirable to extend this very easy — without computers — to handle method to the π mode. It turned out that not only the results are very encouraging — showing that π-like structures behave similarly to $\pi/2$-mode structures — but also the shape of the formulas arrived at is of a surprising beauty. Although the calculations are only applied to deflecting structures, they are also usable for any kind of multiperiodic structure.

II. Equivalent Circuit Analysis

1. The step from $\pi/2$ mode to π mode

In Ref. 1 an equivalent circuit was used which is explained in Figs. 1-3. Figure 1 shows the structure under consideration, the cells being numbered 0, 1, 2 ... have the form of a T, each $\frac{1}{4}\lambda$ long and consist of one cylinder plus one disc plus one cylinder:

---

1. H. Hahn and D.M. Lazarus, BNL Accelerator Dept. Informal Report AADD-186 (1972).
2. J.R. Aggus, W. Bauer, S. Giordano, H. Hahn, and H.J. Halama, in Proc. 1973 Particle Accelerator Conference, San Francisco, March 1973 (in press).

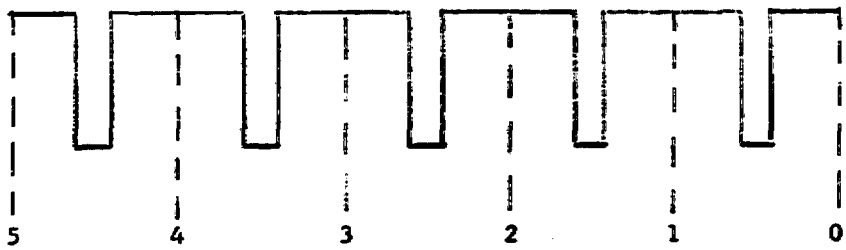

Fig. 1. $\pi/2$ structure.

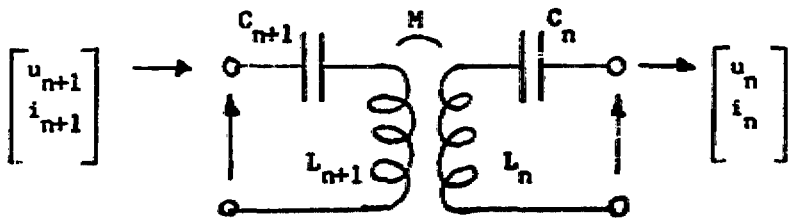

Fig. 2. Equivalent circuit.

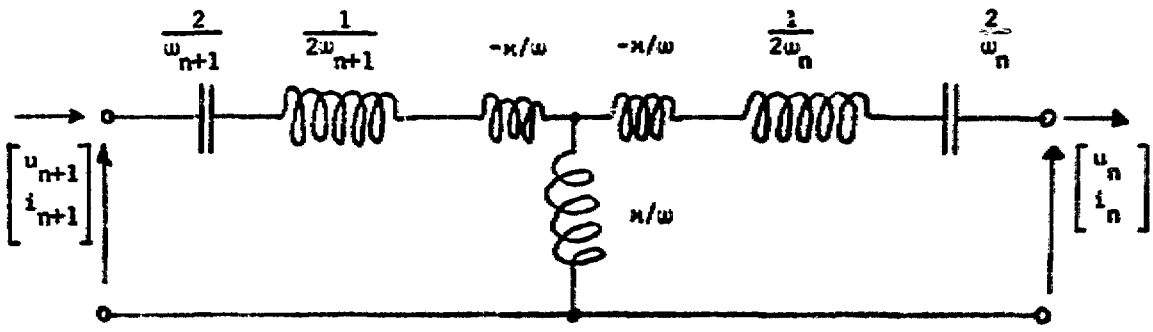

Fig. 3. Equivalent circuit redrawn.

The transfer matrix $T(n+1,n)$, connecting the voltage-current vector at the center of the $(n+1)^{th}$ cell to the nth cell

$$\begin{bmatrix} u_{n+1} \\ i_{n+1} \end{bmatrix} = T(n+1,n) \begin{bmatrix} u_n \\ i_n \end{bmatrix} \tag{1}$$

is in linearized form given by the product

$$\begin{bmatrix} 1 & j(\Omega - \Omega_{n+1} - \kappa) \\ 0 & 1 \end{bmatrix} \begin{bmatrix} 1 & 0 \\ \frac{1}{j\kappa} & 1 \end{bmatrix} \begin{bmatrix} 1 & j(\Omega - \Omega_n - \kappa \\ 0 & 1 \end{bmatrix} \tag{2}$$

with $\Omega = (\omega - \omega_{\pi/2})/\omega_{\pi/2}$ being the relative frequency deviation of the cavity from the unperturbed $\pi/2$ mode, and $\Omega_n = (\omega_n - \omega_{\pi/2})/\omega_{\pi/2}$ being the frequency deviation of the nth cell from the unperturbed $\pi/2$ mode. This product of three matrices represents the cylinder plus disc plus cylinder connected in series as shown in Fig. 1. It is in this form suitable to represent a structure operated in the $\pi/2$ mode, as shown in Ref. 1.

To use the same kind of matrices for the description of a π-mode structure, it will be seen that one only has to write 2κ instead of κ in Eq. (1). For convenience we also change to

$$\varepsilon = \frac{\Omega}{\kappa}, \quad \varepsilon_i = \frac{\Omega_i}{\kappa}$$

and get

$$T(n+1,n) = \begin{bmatrix} 1 & j\kappa(\varepsilon - \varepsilon_{n+1} - 2) \\ 0 & 1 \end{bmatrix} \begin{bmatrix} 1 & 0 \\ \frac{1}{j\kappa} & 1 \end{bmatrix} \begin{bmatrix} 1 & j\kappa(\varepsilon - \varepsilon_n - 2) \\ 0 & 1 \end{bmatrix} \tag{3}$$

The product of these three matrices is the transfer matrix $T^{(1)}$ of one T of the π-mode structure:

$$T^{(1)} = \begin{bmatrix} \varepsilon - \varepsilon_{n+1} - 1 & j\kappa(-2\varepsilon + \varepsilon_n + \varepsilon_{n+1}) \\ \frac{1}{j\kappa} & \varepsilon - \varepsilon_n - 1 \end{bmatrix} \tag{4}$$

For a structure without fabricating tolerances ($\epsilon_i = 0$), $T^{(1)}$ reduces to

$$\begin{bmatrix} \epsilon - 1 & 0 \\ \frac{1}{j\varkappa} & \epsilon - 1 \end{bmatrix} \tag{4a}$$

It can be shown[3] that the dispersion relation follows from the trace of the matrix $T^{(1)}$

$$\cos\varphi = \tfrac{1}{2}\,\mathrm{tr}(T^{(1)}) = \epsilon - 1 \tag{5}$$

For $\epsilon = 0$ follows $\varphi = \pi$, demonstrating that the matrix Eq. (3) is adequate for the description of the π mode.

The numerical value of $\varkappa$ is for the $\pi/2$ mode given by the group velocity $v_g = \pi/2\varkappa$, and in the case of the π mode by the curvature of the experimental dispersion diagram at the operating point:

$$\Omega = \varkappa \cdot \Delta\varphi^2/2 \tag{5a}$$

For the $\pi/2$ mode, we use $v_g = -0.0372$ from Ref. 4, which gives $\varkappa = 0.0237$. For the π mode, a measurement of the dispersion diagram[5] yielded $\varkappa = 0.0126$.

For later use we calculate also a rms value $\bar{\epsilon}_i$ of the individual errors. In Ref. 1 $\bar{\epsilon}_i$ is assumed to be 0.01, using a cavity diameter tolerance

$$\Delta 2b/2b = 25\ \mu\mathrm{m}/128.7\ \mathrm{mm} = 0.195 \times 10^{-3}$$

and a cell length tolerance

$$\Delta h/h = 100\ \mu\mathrm{m}/26.25\ \mathrm{mm} = 0.141 \times 10^{-3}.$$

The formula given there

$$\Omega_i = -\,\Delta b/2b - v_g\,\Delta h/h \tag{5b}$$

reduces for the π mode to $\Omega_i = -\,\Delta 2b/2b$, because $v_g = 0$. Therefore $\bar{\Omega}_i = 0.195 \times 10^{-3}$ and $\bar{\epsilon}_i = 0.0165$. At X-band, $\varkappa$ has the same value, but as the machining tolerance supposedly will not be better than 25 μ, $\bar{\epsilon}_i = 0.05$.

---

3. H. Hahn, BNL Accelerator Dept. Informal Report AADD-139 (1968).
4. W. Bauer, G. Dammertz, H.C. Eschelbacher, H. Hahn, W. Jüngst, E. Rathgeber, and J. Votruba, Proc. 1970 High Energy Instrumentation Conference, Dubna (in press).
5. S. Giordano, private communication.

2. Transfer matrices for more than one T

In order to get the transfer matrix $T^{(2)}$ for two T's, one simply has to multiply two single T's, using the proper indices of the ε_i:

$$T^{(2)} = \begin{bmatrix} \varepsilon - \varepsilon_{n+2} - 1 & j\varkappa(-2\varepsilon + \varepsilon_{n+1} + \varepsilon_{n+2}) \\ \frac{1}{j\varkappa} & \varepsilon - \varepsilon_{n+1} - 1 \end{bmatrix} \begin{bmatrix} \varepsilon - \varepsilon_{n+1} - 1 & j\varkappa(-2\varepsilon + \varepsilon_n + \varepsilon_{n+1}) \\ \frac{1}{j\varkappa} & \varepsilon - \varepsilon_n - 1 \end{bmatrix} \tag{6}$$

In multiplying the elements of the matrices one omits all products ε^2, $\varepsilon\varepsilon_i$ and $\varepsilon_i\varepsilon_j$ and retains only products which are linear in the ε's. This is possible, because we are dealing with small deviations from the π-mode frequency, for which $\varepsilon = 0$. $T^{(2)}$ therefore becomes

$$\begin{bmatrix} -(4\varepsilon - 2\varepsilon_{n+1} - 2\varepsilon_{n+2} - 1) & j\varkappa(-4\varepsilon + \varepsilon_n + 2\varepsilon_{n+1} + 2\varepsilon_{n+2}) \\ \frac{1}{j\varkappa}(+2\varepsilon - 2\varepsilon_{n+1} - 2) & -(4\varepsilon - 2\varepsilon_n - 2\varepsilon_{n+1} - 1) \end{bmatrix} \tag{7}$$

By again multiplying Eq. (7) with another T one gets $T^{(3)}$ and so forth.

Tables I to IV show the shape of the elements $T_{11}^{(m)}$, $T_{12}^{(m)}$, $T_{21}^{(m)}$ and $T_{22}^{(m)}$ and demonstrate the rules of finding them:

TABLE I. $T_{11}^{(m)}$

m	$T_{11}^{(m)}$
1	$\varepsilon - \varepsilon_{n+1} - 1$
2	$-(4\varepsilon - 2\varepsilon_{n+1} - 2\varepsilon_{n+2} - 1)$
3	$9\varepsilon - 2\varepsilon_{n+1} - 4\varepsilon_{n+2} - 3\varepsilon_{n+3} - 1$
4	$-(16\varepsilon - 2\varepsilon_{n+1} - 4\varepsilon_{n+2} - 6\varepsilon_{n+3} - 4\varepsilon_{n+4} - 1)$
5	$25\varepsilon - 2\varepsilon_{n+1} - 4\varepsilon_{n+2} - 6\varepsilon_{n+3} - 8\varepsilon_{n+4} - 5\varepsilon_{n+5} - 1$
6	$-(36\varepsilon - 2\varepsilon_{n+1} - 4\varepsilon_{n+2} - 6\varepsilon_{n+3} - 8\varepsilon_{n+4} - 10\varepsilon_{n+5} - 6\varepsilon_{n+6} - 1)$
⋮	
14	$-(196\varepsilon - 2\varepsilon_{n+1} - \ldots - 26\varepsilon_{n+13} - 14\varepsilon_{n+14} - 1)$
⋮	
28	$-(784\varepsilon - 2\varepsilon_{n+1} - \ldots - 54\varepsilon_{n+27} - 28\varepsilon_{n+28} - 1)$

TABLE II. $T_{12}^{(m)}$

m	$T_{12}^{(m)} \cdot (1/j\varkappa)$
1	$-(2\epsilon - \epsilon_n - \epsilon_{n+1})$
2	$4\epsilon - \epsilon_n - 2\epsilon_{n+1} - \epsilon_{n+2}$
3	$-(6\epsilon - \epsilon_n - 2\epsilon_{n+1} - 2\epsilon_{n+2} - \epsilon_{n+3})$
4	$8\epsilon - \epsilon_n - 2\epsilon_{n+1} - 2\epsilon_{n+2} - 2\epsilon_{n+3} - \epsilon_{n+4}$
5	$-(10\epsilon - \epsilon_n - 2\epsilon_{n+1} - 2\epsilon_{n+2} - 2\epsilon_{n+3} - 2\epsilon_{n+4} - \epsilon_{n+5})$
6	$12\epsilon - \epsilon_n - 2\epsilon_{n+1} - 2\epsilon_{n+2} - 2\epsilon_{n+3} - 2\epsilon_{n+4} - 2\epsilon_{n+5} - \epsilon_{n+6}$
⋮	
14	$28\epsilon - \epsilon_n - 2\epsilon_{n+1} \quad \cdots \quad - 2\epsilon_{n+13} - \epsilon_{n+14}$
⋮	
28	$56\epsilon - \epsilon_n - 2\epsilon_{n+1} \quad \cdots \quad - 2\epsilon_{n+27} - \epsilon_{n+28}$

TABLE III. $T_{21}^{(m)}$

m	$T_{21}^{(m)} \cdot (j\varkappa)$
1	1
2	$2\epsilon - 2\epsilon_{n+1} - 2$
3	$-(8\epsilon - 4\epsilon_{n+1} - 4\epsilon_{n+2} - 3)$
4	$20\epsilon - 6\epsilon_{n+1} - 8\epsilon_{n+2} - 6\epsilon_{n+3} - 4$
5	$-(\underset{\sim}{40}\epsilon - 8\epsilon_{n+1} - 12\epsilon_{n+2} - 12\epsilon_{n+3} - 8\epsilon_{n+4} - \underset{\sim}{5})$
6	$70\epsilon - 10\epsilon_{n+1} - 16\epsilon_{n+2} - 18\epsilon_{n+3} - 16\epsilon_{n+4} - 10\epsilon_{n+5} - 6$
⋮	
14	$910\epsilon - 26\epsilon_{n+1} - 48\epsilon_{n+2} - 66\epsilon_{n+3} - 80\epsilon_{n+4} - 90\epsilon_{n+5} \cdots - 14$
⋮	
28	$7308\epsilon - 54\epsilon_{n+1} - 104\epsilon_{n+2} - \cdots - 28$

TABLE IV. $T_{22}^{(m)}$

m	$T_{22}^{(m)}$
1	$\varepsilon - \varepsilon_n - 1$
2	$-(4\varepsilon - 2\varepsilon_n - 2\varepsilon_{n+1} - 1)$
3	$9\varepsilon - 3\varepsilon_n - 4\varepsilon_{n+1} - 2\varepsilon_{n+2} - 1$
4	$-(16\varepsilon - 4\varepsilon_n - 6\varepsilon_{n+1} - 4\varepsilon_{n+2} - 2\varepsilon_{n+3} - 1)$
5	$25\varepsilon - 5\varepsilon_n - 8\varepsilon_{n+1} - 6\varepsilon_{n+2} - 4\varepsilon_{n+3} - 2\varepsilon_{n+4} - 1$
6	$-(36\varepsilon - 6\varepsilon_n - 10\varepsilon_{n+1} - 8\varepsilon_{n+3} - 6\varepsilon_{n+3} - 4\varepsilon_{n+4} - 2\varepsilon_{n+5} - 1)$
⋮	
14	$-(196\varepsilon - 14\varepsilon_n - 26\varepsilon_{n+1} - \quad \ldots \quad - 2\varepsilon_{n+13} - 1)$
⋮	
28	$-(784\varepsilon - 28\varepsilon_n - 54\varepsilon_{n+1} - \quad \ldots \quad - 2\varepsilon_{n+27} - 1)$

Inspecting Tables I-IV one can easily continue them for any value of m. The factor connected with ε in $T_{21}^{(m)}$ is given by the sum of the underlined numbers in the preceding $T^{(m-1)}$, as shown by the following example:

$$T_{21}^{(6)} = 70\varepsilon - 10\varepsilon_{n+1} \ldots .$$

To find the number 70, take $\underset{\sim}{5} + \underset{\sim}{40} + \underset{\sim}{25}$ from the matrix $T^{(5)}$.

There are two convenient tests available, which allow to look for calculating errors:

a) Compute $T_{11}T_{22} - T_{21}T_{12}$. The determinant of the transfer matrix must have the value 1.

b) If one assumes all the ε_i equal, one must arrive at a structure with no fabrication tolerances that behaves like an undisturbed cavity with $\varepsilon = \varepsilon_i$. All matrix elements in Tables I-IV must therefore reduce to the unperturbed π-mode case, for instance:

$$T_{11}^{(4)} = -(16\varepsilon - (2 + 4 + 6 + 4)\ \varepsilon_i - 1) = 1 \quad . \tag{8}$$

3. Multiperiodic structures to be analyzed

The design of a multiperiodic structure is determined by the length of the hot zone of the UHV furnace to be used for heat treating the sections of the structure. Therefore we assume throughout this paper deflecting cavities assembled from sections of approximately 60-cm length. As a comparison with an existing design of a $\pi/2$-mode deflector[6] we analyze a multiperiodic S-band structure which is shown in Fig. 4.

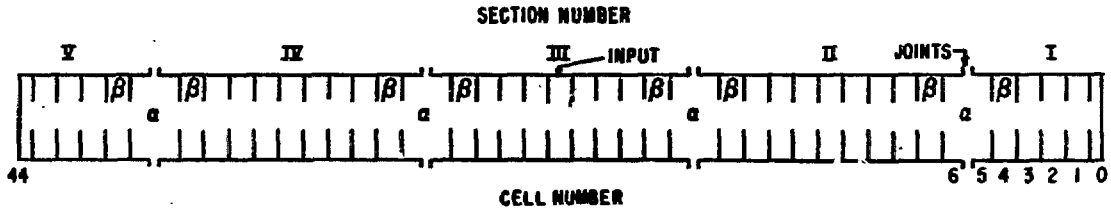

Fig. 4. Multiperiodic π-mode, S-band structure. The 5 sections are represented by the transfer matrices T^{I} - T^{V}. Joints are situated between cells 5 and 6, (16,17), (27,28), (38,39).

The π-mode structure is determined by the operating frequency 2855.1 MHz and the condition $\omega/k = f\lambda = c$. Therefore the cell length has to be 52.5 mm. To form an approximately 60-cm-long section we chose 11 cells/section. (The number of cells has to be odd, in order to provide for a center cell for input coupling.)

The multiperiodic structure is generated by omitting one disc at the location of the joint.[7] Figure 4 anticipates one result of the calculations reported below: Due to the multiperiodicity there appears a gap in the dispersion diagram, which must be closed in order to get a finite group velocity at the π mode — necessary for overcoming the problems of finite fabrication tolerances. It turns out that this gap can only be closed when the end section contains exactly half the number of cells of the middle section. This means that the overall length of the deflector is only 232 cm. By adding two middle sections one can arrive at 347 cm, if necessary.

In addition to the structure of Fig. 4 we analyze an X-band deflector which might be usable with the 200-GeV accelerator at NAL. Again the sections

---

6. W. Bauer, G. Dammertz, H.C. Eschelbacher, H. Hahn, W. Jüngst, E. Rathgeber, J. Votruba, and H. Diepers, IEEE Trans. Nucl. Sci. NS-18, No. 3, 181 (1971).

7. G. Dammertz, thesis Karlsruhe (1973).

should not be longer than 60 cm, but according to the higher frequency the cell length is now 17.3 mm, resulting in middle sections of 33 and end sections of 16½ cells.

4. Transfer matrix of the cells next to the joint

We proceed now by analyzing the part of the cavity shown in Fig. 5.

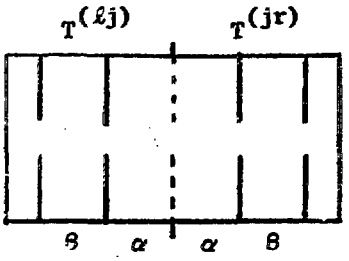

Fig. 5. Cells next to the joint.

At the π mode ($\epsilon \equiv 0$) and without fabricating tolerances ($\epsilon_i = 0$) we demand that, at the location of the omitted disc, the current must be zero. This condition cannot be met by adjusting the cells named α, because these cells are not excited and therefore have very little effect. So one has to adjust the cells named β. As we see later on, we need the α cells for closing the gap. So we now write the transfer matrix $T^{(jr)}$ (right-to-joint) in the same way as Eq. (3) introducing frequency adjustments α and β. The factor 2 appearing in T_{12} of the α and β cells in front of $j\varkappa$ takes into account that their cylinders have twice the length of a regular cylinder:

$$T^{(jr)} = \underbrace{\begin{bmatrix} 1 & 2j\varkappa(-\alpha-2) \\ 0 & 1 \end{bmatrix}}_{\substack{\text{cylinder} \\ \text{frequency} \\ \text{changed by } \alpha}} \underbrace{\begin{bmatrix} 1 & 0 \\ \frac{1}{j\varkappa} & 1 \end{bmatrix}}_{\text{disc}} \underbrace{\begin{bmatrix} 1 & 2j\varkappa(-\beta-2) \\ 0 & 1 \end{bmatrix}}_{\substack{\text{cylinder} \\ \text{frequency} \\ \text{changed by } \beta}} \underbrace{\begin{bmatrix} 1 & 0 \\ \frac{1}{j\varkappa} & 1 \end{bmatrix}}_{\text{disc}} \underbrace{\begin{bmatrix} 1 & -2j\varkappa \\ 0 & 1 \end{bmatrix}}_{\substack{\text{regular} \\ \text{cylinder}}} \tag{9}$$

$$T^{(jr)} = \begin{bmatrix} 4\alpha\beta + 4\alpha + 6\beta + 5 & j\varkappa(-4\alpha\beta - 2\alpha - 6\beta - 2) \\ \frac{1}{j\varkappa}(-2\beta - 2) & 2\beta + 1 \end{bmatrix} \tag{10}$$

$i_{joint} = 0$ means that $T_{22} = 2\beta + 1 = 0$, because the boundary condition at the end plates of the cavity, Fig. 5, requires $u = 0$. β is therefore determined to be

$$\beta = -\frac{1}{2} .$$

$T^{(jr)}$ reduces therefore to

$$T^{(jr)} = \begin{bmatrix} 2(\alpha + 1) & j\varkappa \\ -\frac{1}{j\varkappa} & 0 \end{bmatrix} \tag{11}$$

5. Closing the gap

In the biperiodic structure, one closes the gap by exchanging excited and unexcited cells and equalizing the resonant frequencies.[8] It can be shown that in the multiperiodic structure shown in Fig. 4, the only possible equivalent to this procedure is to equalize the frequencies of the two cavities shown in Fig. 6.

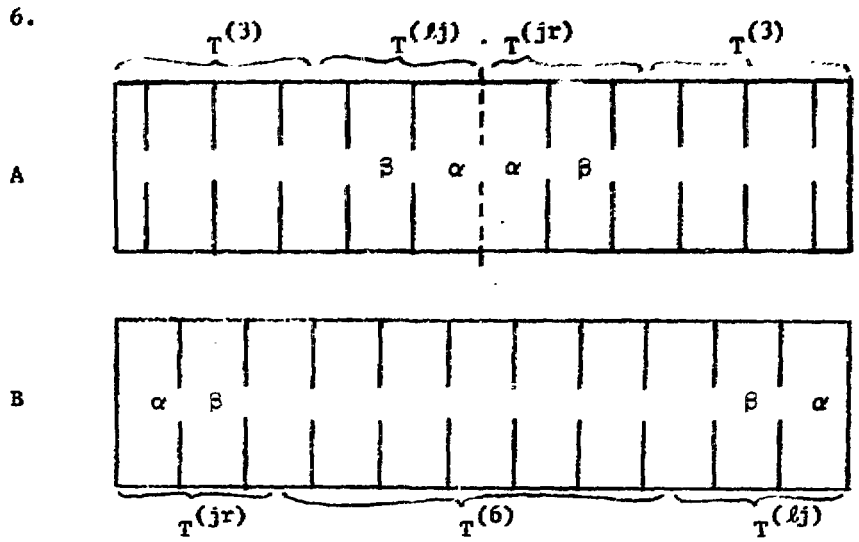

Fig. 6. Two cavities, A and B, whose frequencies must be equal in order to close the gap.

8. W. Bauer, thesis Karlsruhe (1971).

It is this fact that makes it necessary to give the end sections only half the length of the middle sections. We now write the matrices T^A and T^B of both cavities shown in Fig. 6; we set again $\varepsilon_1 \equiv 0$, but we retain ε. With $\beta = -\frac{1}{2}$ we write

$$T^{(jr)} = \begin{bmatrix} 1 & 2j\varkappa(\varepsilon-\alpha-2) \\ 0 & 1 \end{bmatrix} \begin{bmatrix} 1 & 0 \\ \frac{1}{j\varkappa} & 1 \end{bmatrix} \begin{bmatrix} 1 & 2j\varkappa(\varepsilon-\frac{3}{2}) \\ 0 & 1 \end{bmatrix} \begin{bmatrix} 1 & 0 \\ \frac{1}{j\varkappa} & 1 \end{bmatrix} \begin{bmatrix} 1 & j\varkappa(\varepsilon-2) \\ 0 & 1 \end{bmatrix}$$

$$= \begin{bmatrix} -8\varepsilon - 4\alpha\varepsilon + 2\alpha + 2 & j\varkappa(8\varepsilon + 6\alpha\varepsilon + 1) \\ \frac{1}{j\varkappa}(2\varepsilon - 1) & -3\varepsilon \end{bmatrix} \tag{12}$$

Of course, $T^{(\ell j)}$, the matrix "from joint to left" is simply the inverse of $T^{(jr)}$, so we get immediately

$$T^{(\ell j)} = \begin{bmatrix} -3\varepsilon & j\varkappa(8\varepsilon + 6\alpha\varepsilon + 1) \\ \frac{1}{j\varkappa}(2\varepsilon - 1) & -8\varepsilon - 4\alpha\varepsilon + 2\alpha + 2 \end{bmatrix} \tag{13}$$

With these equations (12) and (13), and using Tables I-IV, we can compute

$$T^{(A)} = T^{(3)} \cdot T^{(\ell j)} \cdot T^{(jr)} \cdot T^{(3)} =$$

$$\begin{bmatrix} 18\varepsilon - 36\alpha\varepsilon - 1 & -j\varkappa\, 18\varepsilon \\ \frac{1}{j\varkappa}(44\varepsilon + 160\alpha\varepsilon - 4\alpha + 2) & 18\varepsilon - 36\alpha\varepsilon - 1 \end{bmatrix} \tag{14}$$

and

$$T^{(B)} = T^{(jr)} \cdot T^{(6)} \cdot T^{(\ell j)}$$

$$= \begin{bmatrix} 18\varepsilon - 36\alpha\varepsilon - 1 & j\varkappa(-394\varepsilon + 72\alpha\varepsilon + 72\alpha^2\varepsilon + 4\alpha - 10) \\ -j\varkappa\, 18\varepsilon & 18\varepsilon - 36\alpha\varepsilon - 1 \end{bmatrix} \tag{15}$$

The condition for a closed gap is now the following: The dispersion diagram, as computed by the trace of the matrices Eqs. (14) and (15) $\cos\varphi = \frac{1}{2}(T_{11} + T_{22})$ must show no discontinuity; that means, $\cos\varphi$ must remain real in the vicinity of the π mode ($\cos\varphi = -1$) or $\frac{1}{2}(T_{11} + T_{22})$ must not depend on ε.

So we got the equation for determining α:

$$18\varepsilon - 36\alpha\varepsilon = 0$$
$$\alpha = \tfrac{1}{2} \,. \tag{16}$$

Apparently, $T^{(A)}$ and $T^{(B)}$ lead to the same α, showing that both cavities have the same resonance frequency at the π mode, which was requested above. If one tries to close the gap with structures $T^{(A)}$ and $T^{(B)}$ different from those shown in Fig. 6, one would arrive at a different value of α, and the insertion of additional sections would change this value. Only by making the end sections half as long as the middle sections one α applies for any amount of additional middle sections. Without this property a pretuning of single sections as demonstrated below would be impossible.

6. Transfer matrices of the single sections $T^{(I)} - T^{(V)}$

Having determined α and β, we are now ready to compute the transfer matrices of the sections with fabricating errors ε_i. At first we need again $T^{(jr)}$ and $T^{(\ell j)}$ but now with the ε_i added; for convenience we number the ε_i according to Fig. 7.

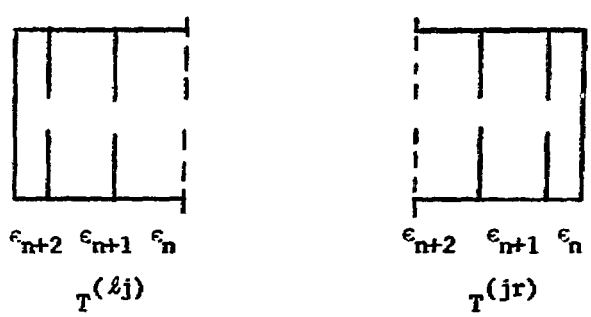

Fig. 7. Numbering the errors ε_i in $T^{(\ell j)}$ and $T^{(jr)}$.

$$T^{(jr)} = \begin{bmatrix} 1 & 2j\varkappa(\varepsilon-\varepsilon_{n+2}-\frac{5}{2}) \\ 0 & 1 \end{bmatrix} \begin{bmatrix} 1 & 0 \\ \frac{1}{j\varkappa} & 1 \end{bmatrix} \begin{bmatrix} 1 & 2j\varkappa(\varepsilon-\varepsilon_{n+1}-\frac{3}{2}) \\ 0 & 1 \end{bmatrix} \begin{bmatrix} 1 & 0 \\ \frac{1}{j\varkappa} & 1 \end{bmatrix} \begin{bmatrix} 1 & j\varkappa(\varepsilon-\varepsilon_n-2) \\ 0 & 1 \end{bmatrix} \tag{17}$$

$$= \begin{bmatrix} -10\varepsilon + 2\varepsilon_{n+2} + 8\varepsilon_{n+1} + 3 & j\varkappa(11\varepsilon - 8\varepsilon_{n+1} - 3\varepsilon_n + 1) \\ \frac{1}{j\varkappa}(2\varepsilon - 2\varepsilon_{n+1} - 1) & -3\varepsilon + 2\varepsilon_{n+1} + \varepsilon_n \end{bmatrix}$$

Again we get $T^{(\ell j)}$ by writing the inverse matrix of $T^{(jr)}$.

$$T^{(\ell j)} = \begin{bmatrix} -3\varepsilon + \varepsilon_{n+2} + 2\varepsilon_{n+1} & j\varkappa(11\varepsilon - 3\varepsilon_{n+2} - 8\varepsilon_{n+1} + 1) \\ \frac{1}{j\varkappa}(2\varepsilon - 2\varepsilon_{n+1} - 1) & (-10\varepsilon + 8\varepsilon_{n+1} + 2\varepsilon_n + 3) \end{bmatrix} \tag{18}$$

$T^{(I)}$, the transfer matrix of the first section is now computed using the numbers of ε_i shown in Fig. 4:

$$T^{(I)} = T^{(jr)} \cdot T^{(3)} \quad . \tag{19}$$

$T^{(II)}$, the transfer matrix of the second section is

$$T^{(II)} = T^{(jr)} \cdot T^{(6)} \cdot T^{(\ell j)} \quad . \tag{20}$$

Tables V-VIII show the elements of the matrices obtained by this procedure.

TABLE V. $T_{11}^{(I)} - T_{11}^{(V)}$

Section	T_{11}
I	$62\varepsilon - 2\varepsilon_5 - 32\varepsilon_4 - 18\varepsilon_3 - 8\varepsilon_2 - 2\varepsilon_1$
II	$8\varepsilon_{15} + 6\varepsilon_{14} + 4\varepsilon_{13} + 2\varepsilon_{12} - 2\varepsilon_{10} - 4\varepsilon_9 - 6\varepsilon_8 - 8\varepsilon_7 - 1$
III	$8\varepsilon_{26} + 6\varepsilon_{25} + 4\varepsilon_{24} + 2\varepsilon_{23} - 2\varepsilon_{21} - 4\varepsilon_{20} - 6\varepsilon_{19} - 8\varepsilon_{18} - 1$
IV	$8\varepsilon_{37} + 6\varepsilon_{36} + 4\varepsilon_{35} + 2\varepsilon_{34} - 2\varepsilon_{32} - 4\varepsilon_{31} - 6\varepsilon_{30} - 8\varepsilon_{29} - 1$
V	$9\varepsilon - 2\varepsilon_{40} - 2\varepsilon_{41} - 2\varepsilon_{42} - 2\varepsilon_{43} - \varepsilon_{44}$

TABLE VI. $T_{12}^{(I)} - T_{12}^{(V)}$

Section	$T_{12}/(j\kappa)$
I	$-20\epsilon + 8\epsilon_4 + 6\epsilon_3 + 4\epsilon_2 + 2\epsilon_1 - 1$
II	$-124\epsilon + 2\epsilon_{16} + 32\epsilon_{15} + 18\epsilon_{14} + 8\epsilon_{13} + 2\epsilon_{12} + 2\epsilon_{10} + 8\epsilon_9 + 18\epsilon_8 + 32\epsilon_7 + 2\epsilon_6$
III	$-124\epsilon + 2\epsilon_{27} + 32\epsilon_{26} + 18\epsilon_{25} + 8\epsilon_{24} + 2\epsilon_{23} + 2\epsilon_{21} + 8\epsilon_{20} + 18\epsilon_{19} + 32\epsilon_{18} + 2\epsilon_{17}$
IV	$-124\epsilon + 2\epsilon_{38} + 32\epsilon_{37} + 18\epsilon_{36} + 8\epsilon_{35} + 2\epsilon_{34} + 2\epsilon_{32} + 8\epsilon_{31} + 18\epsilon_{30} + 32\epsilon_{29} + 2\epsilon_{27}$
V	$-20\epsilon + 2\epsilon_{43} + 4\epsilon_{42} + 6\epsilon_{41} + 8\epsilon_{40} - 1$

TABLE VII. $T_{21}^{(I)} - T_{21}^{(V)}$

Section	$T_{21}\cdot(j\kappa)$
I	$-20\epsilon + 8\epsilon_4 + 6\epsilon_3 + 4\epsilon_2 + 2\epsilon_1 + 1$
II	$18\epsilon - 2(\epsilon_{15} + \ldots + \epsilon_7)$
III	$18\epsilon - 2(\epsilon_{26} + \ldots + \epsilon_{18})$
IV	$18\epsilon - 2(\epsilon_{37} + \ldots + \epsilon_{29})$
V	$-20\epsilon + 2\epsilon_{43} + 4\epsilon_{42} + 6\epsilon_{41} + 8\epsilon_{40} + 1$

TABLE VIII. $T_{22}^{(I)} - T_{22}^{(V)}$

Section	T_{22}
I	$9\epsilon - 2\epsilon_4 - 2\epsilon_3 - 2\epsilon_2 - 2\epsilon_1 - \epsilon_0$
II	$-8\epsilon_{15} - 6\epsilon_{14} - 4\epsilon_{13} - 2\epsilon_{12} + 2\epsilon_{10} + 4\epsilon_9 + 6\epsilon_8 + 8\epsilon_7 - 1$
III	$-8\epsilon_{26} - 6\epsilon_{25} - 4\epsilon_{24} - 2\epsilon_{23} + 2\epsilon_{21} + 4\epsilon_{20} + 6\epsilon_{19} + 8\epsilon_{18} - 1$
IV	$-8\epsilon_{37} - 6\epsilon_{36} - 4\epsilon_{35} - 2\epsilon_{34} - 2\epsilon_{32} + 4\epsilon_{31} + 6\epsilon_{30} + 8\epsilon_{29} - 1$
V	$62\epsilon - 2\epsilon_{43} - 8\epsilon_{42} - 18\epsilon_{41} - 32\epsilon_{40} - 2\epsilon_{39}$

7. Joint-currents of an unpretuned cavity

According to Eq. (1) the current $i_{5,6}$ across the joint between cells 5 and 6 (Fig. 4) is given by

$$i_{5,6} = T_{22}^{(I)} i_o = T_{22}^{(I)} \tag{21}$$

because $u_o = 0$ by boundary conditions and i_o is set to equal 1. The currents at the remaining joints are computed to

$$\begin{aligned} i_{16,17} &= T_{22}^{(II+I)} \\ i_{27,28} &= T_{22}^{(III+II+I)} \\ i_{38,39} &= T_{22}^{(IV+III+II+I)} \end{aligned} \tag{22}$$

$T^{(II+I)}$ being the product $(T^{II}T^{I})$ and so on. These matrix multiplications have been carried out, yielding the results:

$$\begin{aligned} i_{5,6} &= 9\epsilon - \epsilon_o - 2\sum_{1}^{4} \epsilon_i \\ i_{16,17} &= -27\epsilon + \epsilon_o + 2\sum_{1}^{4} \epsilon_i + 2\sum_{7}^{15} \epsilon_i \\ i_{27,28} &= 45\epsilon - \epsilon_o - 2\sum_{1}^{4} \epsilon_i - 2\sum_{7}^{15} \epsilon_i - 2\sum_{18}^{26} \epsilon_i \\ i_{38,39} &= -63\epsilon + \epsilon_o + 2\sum_{1}^{4} \epsilon_i + 2\sum_{7}^{15} \epsilon_i + 2\sum_{18}^{27} \epsilon_i + 2\sum_{29}^{37} \epsilon_i \end{aligned} \tag{23}$$

The boundary condition $u_o = u_{44} = 0$ at both endplates of the whole cavity demands that T_{12} of the overall transfer matrix

$$T = T^{V}\, T^{IV}\, T^{III}\, T^{II}\, T^{I} \tag{24}$$

must be zero. T_{12} happens to equal

$$T_{12} = 0 = j\varkappa \left(72\varepsilon - \varepsilon_o - 2 \sum_{\substack{1-4\\7-15\\18-26\\29-37\\40-43}} \varepsilon_i - \varepsilon_{44}\right) \tag{25}$$

The effect of the fabrication errors ε_i is therefore a change of the resonant frequency which is given by Eq. (25):

$$\varepsilon = \left(\varepsilon_o + 2 \sum_{\substack{1-4\\7-15\\18-26\\29-37\\40-43}} \varepsilon_i + \varepsilon_{44}\right) / 72 \tag{26}$$

Introducing Eq. (26) into Eqs. (23) yields the final expressions for the untuned joint-currents:

$$i_{5,6} = -\frac{7}{8}\left(\varepsilon_o + 2 \sum_{1-4} \varepsilon_i\right) + \frac{1}{8}\left(2 \sum_{\substack{7-15\\18-26\\29-37\\40-43}} \varepsilon_i + \varepsilon_{44}\right)$$

$$i_{16,17} = \frac{5}{8}\left(\varepsilon_o + 2 \sum_{\substack{1-4\\7-15}} \varepsilon_i\right) - \frac{3}{8}\left(2 \sum_{\substack{18-26\\29-37\\40-43}} \varepsilon_i + \varepsilon_{44}\right)$$

$$i_{27,28} = -\frac{3}{8}\left(\varepsilon_o + 2 \sum_{\substack{1-4\\7-15\\18-26}} \varepsilon_i\right) + \frac{5}{8}\left(2 \sum_{\substack{29-32\\40-43}} \varepsilon_i + \varepsilon_{44}\right) \tag{27}$$

$$i_{38,39} = \frac{1}{8}\left(\varepsilon_o + 2 \sum_{\substack{1-4\\7-15\\18-26\\29-37}} \varepsilon_i\right) - \frac{7}{8}\left(2 \sum_{40-43} \varepsilon_i + \varepsilon_{44}\right)$$

To compute the mean square value of the joint-currents according to Eqs. (27) using one mean value of the ϵ_i, $\bar{\epsilon}_i$ one has to add the squares of the factors appearing in Eqs. (27), for instance

$$i_{5,6} = \bar{\epsilon}_i \sqrt{\left(\frac{7}{8}\right)^2 + \left(\frac{7}{8} \cdot 2\right)^2 \cdot 4 + \left(\frac{1}{8} \cdot 2\right)^2 \cdot 31 + \left(\frac{1}{8}\right)^2} \tag{28}$$

Table IX shows the results obtained so far.

8. Pretuning the sections

Pretuning a $\pi/2$-mode section is accomplished by attaching only one error-free T at each joint and changing the overall frequency by, say, electropolishing the section until the desired frequency is reached within a certain range. Unfortunately, for the multiperiodic structure we need two "error free" parts of the size of section I and section V. These sections may be made from copper-plated invar and must be tuned by very careful measurements. Using these two sections one can again tune the niobium sections by electropolishing. The results are computed in the following.

We assume a section $\underset{\sim}{T}^{(V)}$ in which all $\epsilon_i \equiv 0$, and form a cavity

$$\underset{\sim}{T} = \underset{\sim}{T}^{(V)} \, T^{(I)} \tag{29}$$

Again, $\underset{\sim}{T}_{12}$ must equal zero as before and we get

$$\underset{\sim}{T}_{12} = j\kappa \left(18\epsilon - 2\sum_1^4 \epsilon_i - \epsilon_o\right) = 0 \tag{30}$$

or

$$\epsilon^I = \epsilon = \left(2\sum_1^4 \epsilon_i + \epsilon_o\right) / 18 \quad . \tag{31}$$

$\epsilon^I = 0$ would mean that the first section was perfectly tuned. In practice, ϵ^I is the tuning error of the first section.

TABLE IX. Comparison of Various Deflecting Structures.

Mode	$\pi/2$	Multiperiodic*	Multiperiodic*
Frequency (GHz)	2.855	2.855	8.6
Overall Length (cm)	273	232 (347)	229 (343)
Number of cells,† end sections	2 x 19	2 x 5½	2 x 16½
Number of cells, middle sections	3 x 22	3 x 11 (5 x 11)	3 x 33 (5 x 33)
Cell length (mm)	26.25	52.5	17.3
Iris thickness (mm)	10	20	6.7
Iris hole diameter (mm)	40	40	13.3
Magnetic field ratio H_p/E_o (G/MV/m)	158	118	118
Electric field ratio E_p/E_o	5.6	3.3	3.3
H_p (G)	400	400	400
E_o (MV/m)	2.53	3.40	3.4
Transverse momentum per deflector (MeV/c)	7.0	6.4 (9.6)	7.3 (11)
$(R/Q)_{theory}$ (Ω/m)	847.5	1150	3480
Q_{theory} (Cu, 300 K)	10 300	15 600	9000
Improvement factor	5×10^4	5×10^4	10^5
Power per deflector (W)	25	15 (22)	7.9 (12)
Currents at joints (not pretuned):			
i_1	5.5 $\bar{\epsilon}_i$	3.9 $\bar{\epsilon}_i$ (4.0 $\bar{\epsilon}_i$)	7.2 $\bar{\epsilon}_i$ (7.5 $\bar{\epsilon}_i$)
i_2	7.0 $\bar{\epsilon}_i$	5.7 $\bar{\epsilon}_i$ (6.4 $\bar{\epsilon}_i$)	13.7 $\bar{\epsilon}_i$ (11.7 $\bar{\epsilon}_i$)
i_3		(7.1 $\bar{\epsilon}_i$)	(13.4 $\bar{\epsilon}_i$)
Currents at joints (pretuned):			
i_1	18.4 $\bar{\epsilon}^m$	17.7 $\bar{\epsilon}^m$ (17.9 $\bar{\epsilon}^m$)	61.0 $\bar{\epsilon}^m$ (77.0 $\bar{\epsilon}^m$)
i_2	24.5 $\bar{\epsilon}^m$	35.5 $\bar{\epsilon}^m$ (35.5 $\bar{\epsilon}^m$)	111.4 $\bar{\epsilon}^m$ (109.5 $\bar{\epsilon}^m$)
i_3		(41.5 $\bar{\epsilon}^m$)	(111.0 $\bar{\epsilon}^m$)

*In parenthesis: version with 7 sections.

†1 cell = ¼ wavelength in $\pi/2$, ½ wavelength in π mode.

In the same way one gets

$$\begin{aligned}
\varepsilon^{II} &= \left(2\sum_{7}^{15} \varepsilon_i\right) / 36 \\
\varepsilon^{III} &= \left(2\sum_{18}^{36} \varepsilon_i\right) / 36 \\
\varepsilon^{IV} &= \left(2\sum_{29}^{37} \varepsilon_i\right) / 36 \\
\varepsilon^{V} &= \left(2\sum_{40}^{43} \varepsilon_i + \varepsilon_{44}\right) / 18
\end{aligned} \tag{32}$$

Introducing these section tuning errors into Eqs. (27) yields the joint-currents for a pretuned cavity:

$$\begin{aligned}
i_{5,6} &= \frac{9}{4}\,(-\,7\varepsilon^{I} + 2\varepsilon^{II} + 2\varepsilon^{III} + 2\varepsilon^{IV} + \varepsilon^{V}) \\
i_{16,17} &= \frac{9}{4}\,(\;\;5\varepsilon^{I} + 10\varepsilon^{II} - 6\varepsilon^{III} - 6\varepsilon^{IV} - 3\varepsilon^{V}) \\
i_{27,28} &= \frac{9}{4}\,(-\,3\varepsilon^{I} - 6\varepsilon^{II} - 6\varepsilon^{III} + 10\varepsilon^{IV} + 5\varepsilon^{V}) \\
i_{38,39} &= \frac{9}{4}\,(\;\;\varepsilon^{I} + 2\varepsilon^{II} + 2\varepsilon^{III} + 2\varepsilon^{IV} - 7\varepsilon^{V})
\end{aligned} \tag{33}$$

The numerical results given in Table IX again are the mean square values as shown above.

An rms value for the ε^m is obtained by the assumption that one possibly can tune an S-band section to 30 kHz. Using $\varkappa = 0.0126$ (Eq. 5a) yields $\bar{\varepsilon}^m \approx 10^{-3}$. At X-band again a factor of 3 gives $\bar{\varepsilon}^m = 3 \times 10^{-3}$.

9. Corrections to Reference 1

In order to compare the above results with those given in Ref. 1 for the $\pi/2$ mode, a correction of an error is necessary as pointed out by Jüngst.[9]

---

9. W. Jüngst, External Report 3/72-4, Kernforschungszentrum Karlsruhe (1972), to be published.

Using the same procedure as shown above, one finds that Eqs. (12a) in Ref. 1 must read

$$\epsilon^{I} = \left(2 \sum_{2^e}^{18} \epsilon_i + \epsilon_o\right) / 20$$

$$\epsilon^{II} = \left(2 \sum_{20^e}^{40} \epsilon_i\right) / 24$$

$$\epsilon^{III} = \left(2 \sum_{42^e}^{62} \epsilon_i\right) / 24$$

$$\epsilon^{IV} = \left(2 \sum_{64^e}^{84} \epsilon_i\right) / 24$$

$$\epsilon^{V} = \left(2 \sum_{86^e}^{102} \epsilon_i + \epsilon_{104}\right) / 20$$

Using these expressions, Eqs. (14) become

$$i_{19} = -\frac{425}{26}\epsilon^{I} + \frac{57}{13}(\epsilon^{II} + \epsilon^{III} + \epsilon^{IV}) + \frac{95}{26}\epsilon^{V}$$

$$i_{41} = -\frac{315}{26}\epsilon^{I} - \frac{189}{13}\epsilon^{II} + \frac{123}{13}(\epsilon^{III} + \epsilon^{IV}) + \frac{205}{26}\epsilon^{V}$$

$$i_{63} = -\frac{205}{26}\epsilon^{I} - \frac{123}{13}(\epsilon^{II} + \epsilon^{III}) + \frac{189}{13}\epsilon^{IV} + \frac{315}{26}\epsilon^{V}$$

$$i_{85} = -\frac{95}{26}\epsilon^{I} - \frac{57}{13}(\epsilon^{II} + \epsilon^{III} + \epsilon^{IV}) + \frac{425}{26}\epsilon^{V} \quad .$$

10. Analysis of a π-mode X-band deflector

We turn now to an X-band deflector with cell length 17.3 mm, middle sections of 33 cells and end cells of 16½ cells. Table X gives the necessary information on numbers and indices:

TABLE X

Section	Cell Number	Joint-Current
$T^{(I)}$	0 - 16	$i_{16,17}$
$T^{(II)}$	17 - 49	$i_{49,50}$
$T^{(III)}$	50 - 82	$i_{82,83}$
$T^{(IV)}$	83 - 115	$i_{115,116}$
$T^{(V)}$	116 - 132	

To analyze this structure, it is not necessary to repeat all the steps shown above: Although it is clear that α [Eq. (9)] will be changed, because $T^{(A)}$ and $T^{(B)}$, Eqs. (14) and (15) are different, it is easy to show that the value of α has no influence on the currents. If one traces back the origin of the number 72 in Eq. (25) one states that it comes from the 9 in $T_{11}^{(5)} = 9\epsilon - \ldots$ and from the 9 in $T_{22}^{(1)} = 9\epsilon - \ldots$. Furthermore, these two 9 are the sum of the 3 in $T_{22}^{(jr)} = -3\epsilon$ and the 6 in $T_{12}^{(3)} = -6\epsilon + \ldots$. All these numbers are not influenced by α. So one can immediately substitute instead of 9 = 6 + 3, and 9 + 18 + 18 + 18 + 9 = 72 for the X-band structure 31 = 28 + 3, and 31 + 62 + 62 + 62 + 31 = 248. Therefore, Eq. (26) reads now

$$\epsilon = \left(\epsilon_o + 2 \sum_{\substack{1-15\\18-48\\51-81\\84-114\\116-131}} \epsilon_i + \epsilon_{132}\right) / 248 \quad . \tag{34}$$

In the same way one finds the currents by analogue guessing and finally gets, that Eqs. (27) remain unchanged except for the summation indices and some signs:

$$i_{16,17} = \frac{7}{8}\left(\epsilon_o + 2\sum_{1-15} \epsilon_i\right) - \frac{1}{8}\left(2\sum_{\substack{18-48\\51-41\\84-114\\116-131}} \epsilon_i + \epsilon_{132}\right)$$

$$i_{49,50} = -\frac{5}{8}\left(\epsilon_o + 2\sum_{\substack{1-15\\18-48}} \epsilon_i\right) + \frac{3}{8}\left(2\sum_{\substack{51-81\\84-114\\116-131}} \epsilon_i + \epsilon_{132}\right) \tag{35}$$

and so on. The expressions for the pretuning errors now become

$$\epsilon^{I} = \left(\epsilon_o + 2\sum_{1-15} \epsilon_i\right) / 62$$

$$\epsilon^{II} = \left(2\sum_{18-48} \epsilon_i\right) / 124$$

$$\epsilon^{III} = \left(2\sum_{51-81} \epsilon_i\right) / 124 \tag{36}$$

$$\epsilon^{IV} = \left(2\sum_{84-114} \epsilon_i\right) / 124$$

$$\epsilon^{V} = \left(2\sum_{117}^{131} \epsilon_i + \epsilon_{132}\right) / 62$$

and finally the joint-currents for the pretuned X-band cavity are

$$i_{16,17} = \frac{31}{4}\left(7\epsilon^{I} - 2\epsilon^{II} - 2\epsilon^{III} - 2\epsilon^{IV} - \epsilon^{V}\right)$$

$$i_{49,50} = \frac{31}{4}\left(-5\epsilon^{I} - 10\epsilon^{II} + 6\epsilon^{III} + 6\epsilon^{IV} + 3\epsilon^{V}\right) \tag{37}$$

and similar $i_{82,83}$, $i_{115,116}$. Table IX includes the numerical results.

11. Analysis of cavities with 7 sections at S-band and X-band

Looking in Table IX at the overall deflections obtained by the cavities analyzed so far, one might prefer to have a somewhat longer cavity. Unfortunately,

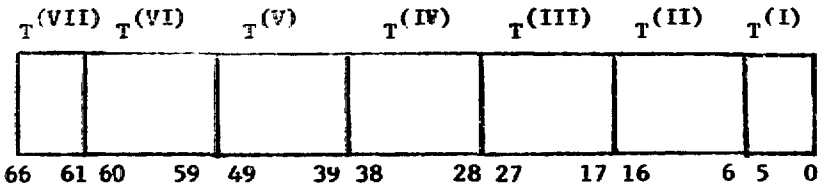

Fig. 8. Multiperiodic S-band structure with 7 sections represented by the transfer matrices $T^{(I)}$-$T^{(VII)}$. Joints are located between cells 5,6, 16,17, 27,28, 38,39, 49,50, 60,61.

because of symmetry considerations, one can only add two middle sections. In the following we briefly check, how the expressions derived above change, when the S-band structure shown in Fig. 8 is used. All we have to do now is to add two more middle section transfer matrices to Tables V-VIII and give the ϵ_i of the last section, T^{VII}, the proper indices. By multiplying these single matrices as in Eq. (22) one gets

$$\epsilon = \Big(\epsilon_o + 2 \sum_{\substack{1-4\\7-15\\18-26\\29-37\\40-48\\51-59\\62-65}} \epsilon_i + \epsilon_{66}\Big) / 108 \quad , \tag{38}$$

and the untuned joint-currents become

$$i_{5,6} = -\frac{11}{12}\Big(\epsilon_o + 2 \sum_{1-4} \epsilon_i\Big) + \frac{1}{12}\Big(2 \sum_{\substack{7-15\\18-26\\29-37\\40-48\\51-59\\62-65}} \epsilon_i + \epsilon_{66}\Big)$$

$$i_{16,17} = \frac{3}{4}\Big(\epsilon_o + \sum_{\substack{1-4\\7-15}} \epsilon_i\Big) - \frac{1}{4}\Big(2 \sum_{\substack{18-26\\29-37\\40-48\\51-59\\62-65}} \epsilon_i + \epsilon_{66}\Big) \tag{39}$$

$$i_{27,28} = -\frac{7}{12}\Big(\epsilon_o + 2 \sum_{\substack{1-4\\7-15\\18-26}} \epsilon_i\Big) + \frac{5}{12}\Big(2 \sum_{\substack{29-37\\40-48\\51-59\\62-65}} \epsilon_i + \epsilon_{66}\Big)$$

and similar $i_{38,39}$, $i_{49,50}$ and $i_{60,61}$.

Table XI shows the coefficients entering into the untuned joint-currents for the several configurations considered so far, leading obviously to the assumption for 7 sections — X-band which is also shown in the table.

TABLE XI. Coefficients entering the expressions for the untuned joint-currents.

Joint Number	4 joints S-band		6 joints S-band		4 joints X-band		6 joints X-band	
	Eq. (27)		Eq. (39)		Eq. (35)		Deduced	
1	-7/8	1/8	-11/12	1/12	7/8	-1/8	11/12	-1/12
2	5/8	-3/8	9/12	-3/12	-5/8	3/8	9/12	3/12
3	-3/8	5/8	-7/12	5/12	3/8	-5/8	7/12	-5/12
4	1/8	-7/8	5/12	-7/12	1/8	7/8	5/12	7/12
5			-3/12	9/12			3/12	-9/12
6			1/12	-11/12			-1/12	11/12

Finally one arrives at the pretuned joint-currents, for S-band:

$$
\begin{aligned}
i_{5,6} &= \frac{9}{6}\left[-11\epsilon^{I} + 2(\epsilon^{II} + \epsilon^{III} + \epsilon^{IV} + \epsilon^{V} + \epsilon^{VI}) + \epsilon^{VII}\right] \\
i_{16,17} &= \frac{9}{6}\left[9\epsilon^{I} + 18\epsilon^{II} - 6(\epsilon^{III} + \epsilon^{IV} + \epsilon^{V} + \epsilon^{VI}) + 3\epsilon^{VII}\right] \qquad (40) \\
i_{27,28} &= \frac{9}{6}\left[-7\epsilon^{I} - 14(\epsilon^{II} + \epsilon^{III}) + 10(\epsilon^{IV} + \epsilon^{V} + \epsilon^{VI}) + 5\epsilon^{VII}\right]
\end{aligned}
$$

again the remaining currents resulting in the same numerical values, and for X-band:

$$
\begin{aligned}
i_{16,17} &= \frac{31}{6}\left[11\epsilon^{I} - 2(\epsilon^{II} + \ldots \epsilon^{VI}) - \epsilon^{VII}\right] \\
i_{49,50} &= \frac{31}{6}\left[-9\epsilon^{I} - 18\epsilon^{II} + 6(\epsilon^{III} + \ldots \epsilon^{VI}) + 3\epsilon^{VII}\right] \qquad (41) \\
i_{82,83} &= \frac{31}{6}\left[7\epsilon^{I} + 14(\epsilon^{II} + \epsilon^{III}) - 10(\epsilon^{IV} + \ldots \epsilon^{VI}) - 5\epsilon^{VII}\right]
\end{aligned}
$$

The $\epsilon^{I} \ldots \epsilon^{VII}$ appearing in Eqs. (40) and (41) are the same as in Eqs. (32) and (36) respectively.

III. Conclusions

In Table IX the calculations described above are applied to compare several deflecting structures. The values of shunt impedance, Q, H_p/E_o and E_p/E_o are taken from Vaghin[10] and, of course, scaled to the required frequency where necessary.

In the first two rows the $\pi/2$-mode, S-band deflector presently under construction at Karlsruhe[6] is compared with the multiperiodic structure shown in Fig. 4. The somewhat surprising result of the calculations is that the joint-currents are of the same order of magnitude in the multiperiodic structure. Considering the other quantities entering Table IX one concludes that a multiperiodic structure of 2.32 m length gives only slightly less deflection than a $\pi/2$-mode structure of 2.73 m, but needs a smaller cryostat and will surely be cheaper, because it needs only half the number of cells and electron-beam welds. In addition, the possibility of multipactoring is considerably reduced by the larger distance of the discs and the lower E_p/E_o ratio of the π mode.

In the case of an X-band separator the discs of a $\pi/2$-mode deflector would become very thin and narrow. So not only the higher shunt impedance and the lower peak field ratios, but also simple geometrical considerations would favor the π mode. Since joints are unavoidable, the problem of joint-currents as function of fabrication tolerances had to be solved. Although the computed joint-currents shown in Table IX for the X-band deflector are higher than those in the S-band deflector, we are quite sure that an X-band deflector for use at high particle momenta is possible in principle. In addition, as shown in Ref. 11, at X-band one probably would choose a larger iris aperture, thus reducing the joint-currents by an increased $\varkappa$.

Acknowledgement

I would like to thank Dr. Harald Hahn for his continuing support during the preparation of the above paper. Without his ideas and without discussing with him every step it would not have been completed.

---

10. V. Vaghin, CERN Report 71-4 (1971).
11. W. Bauer, BNL Accelerator Dept. Internal Report AADD 73-4 (1973).

Distr.: AADD Limited